JRC2018-6141

RAILROAD RAILS CONTAINING ELECTRODE-INDUCED PITTING FROM PRESSURE ELECTRIC WELDING

Blain R. Luck
Federal Railroad Administration
U.S. Department of Transportation
Bismarck, ND, USA

Gregory N. Vigilante
Christopher L. Ethier
Edward J. Troiano
Benét Laboratories
U.S. Army
Watervliet, NY, USA

Brian Marquis
Hailing Yu
David Y. Jeong[1]
Volpe National Transportation Systems Center
U.S. Department of Transportation
Cambridge, MA, USA

ABSTRACT

The Federal Railroad Administration (FRA) routinely conducts investigations of railroad accidents to determine causation and any contributing factors to help the railroad industry implement corrective measures that may prevent similar incidents in the future. Over the past decade, FRA has investigated multiple broken rail accidents in which fractures in the rail web were identified. The common features observed in the recovered rail fragments from these accidents included welds and spots or burn marks on the web, indicating that the rails were joined together by pressure electric welding.

Pressure electric welding uses a welding head that clamps around two opposing rail ends, pressing an electrode on each rail, then hydraulically pulling the rail ends together while arcing current through the electrodes into the rails, causing them to essentially melt together to form a continuous rail.

Based on the similarities observed in the web fractures, FRA rail integrity specialists hypothesized that stray (i.e. inadvertent and unwanted) arcing during pressure electric welding can result in the formation of burns or pits on the rail where it makes contact with the electrodes. Moreover, these electrode-induced pits behave as stress raisers (also referred to as stress concentrations). Fatigue cracks often develop at locations of stress concentration. Once a fatigue crack initiates, the localized stress encourages the growth of the crack, which may potentially lead to rail failure.

This paper describes the forensic evaluations of three railroad rails containing electrode-induced pitting. These evaluations include: magnetic particle inspection to nondestructively detect cracks emanating from the pitting; fractography to study the fracture surfaces of the cracks; metallography to study the microstructure; analysis of chemical composition; and measurements of tensile mechanical properties and fracture toughness of rail steel. Moreover, the results of these evaluations confirm the hypothesis postulated by FRA that stray arcing during pressure electric welding can cause electrode-induced pitting.

INTRODUCTION

Figure 1 shows a photograph of a rail with electrode pits in the web. The location of these electrode pits, when they occur, is typically four to eight inches on either side of the weld. Electrode-induced pitting from pressure electric welding may also occur in the head and base of the rail. It is unclear whether traditional ultrasonic rail testing can consistently detect electrode-induced pitting.
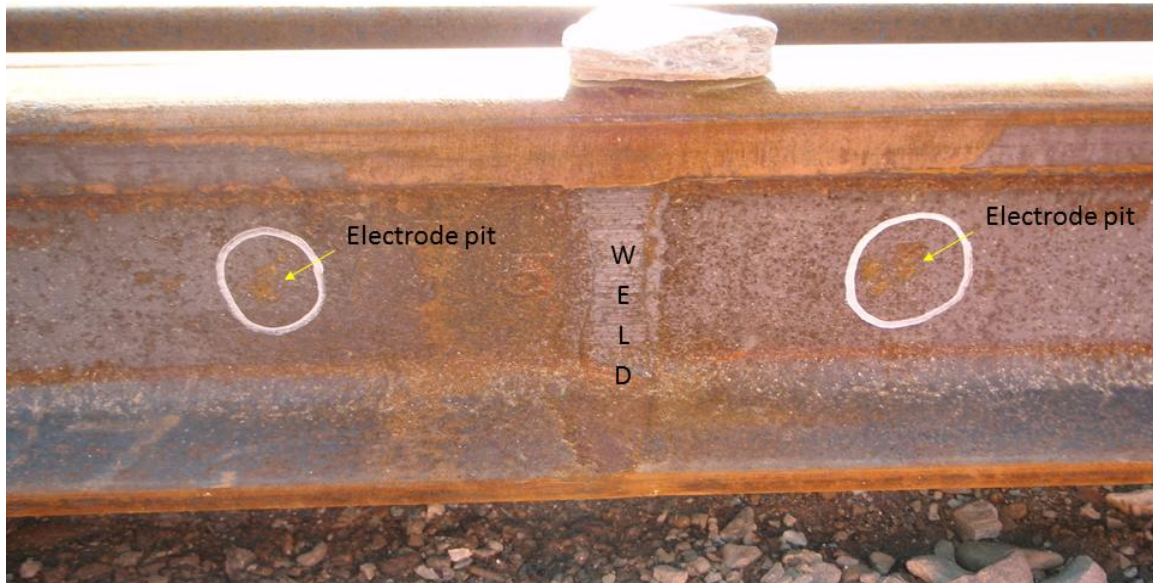
---

[1] Retired

Figure 1: Electrode Pits on the Web of a Railroad Rail

In 2016, FRA's Office of Railroad Safety requested technical support from the Volpe National Transportation Systems Center (Volpe) to study the fatigue and fracture behavior of rails with electrode-induced pitting from pressure electric welding. Volpe has been providing FRA with technical support in track systems safety research, which includes rail integrity, for the past four decades. In addition, Volpe provides FRA with technical assistance in accident investigations on an ad-hoc basis.

The Federal Laboratory Consortium (FLC) is a nationwide network of federal laboratories, agencies, and research centers that was formed to promote and facilitate technology transfer. Volpe and the U.S. Army's Benét Laboratories (Benét) are members of the FLC network. Moreover, Benét has technical capabilities and expertise in analysis and testing of materials that are applicable to the examination of railroad rail steel. Consequently, Volpe enlisted technical support from Benét, through an Inter-agency Agreement, to conduct forensic examinations of three rail sections with electrode-induced pitting in the web from the pressure electric welding process, which were obtained by FRA from members of the railroad industry.

This paper describes the forensic evaluations performed by Benét, and summarizes the results. A more detailed description of the methods used in these evaluations, as well as more detailed results, can be found in Reference [1].
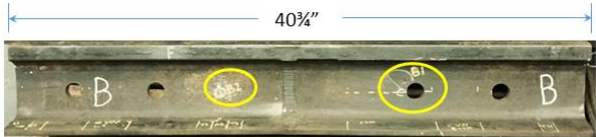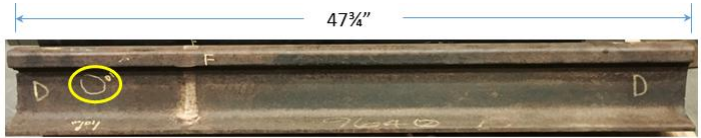
BENÉT EVALUATIONS

Benét's evaluations began with visual examinations of the three rails. Table 1 summarizes the general characteristics of three rails (designated as Rails B, C, and D) obtained by FRA for forensic evaluation. The locations of the electrode burn marks on each rail are highlighted by yellow ellipses.

Magnetic particle inspection (MPI), a nondestructive testing method, was conducted to confirm and identify the presence of any cracks. Figure 2 shows three images of specific features in each of the rails identified from MPI. MPI clearly identified a through-web crack in feature B1 of Rail B, which also runs through the electrode pit. MPI also identified indications in Rails C and D, as shown in Figure 2.

The rails were then sectioned or cut into several specimens for the following specific forensic evaluations: fractography (the science of studying fracture surfaces to identify the origin and causes of fracture), metallography (the science of studying the microstructure of metals to provide information concerning the properties and processing history of metallic alloys), and testing to determine the chemical composition, tensile mechanical properties, hardness, and impact resistance of the rail steel. Subsequent evaluations included fracture toughness testing and residual stress measurements. Figure 3 shows a schematic diagram of the evaluations performed on each rail. For example, all of the evaluations were performed on Rail B except the fracture toughness residual stress measurements. All of the evaluations were conducted on Rail D except fractography, tensile testing, and impact testing.

**Table 1: Summary of Rails Evaluated in Forensic Examinations**

Rail ID	Rail Section	Manufacturer	Year	Comments
B	115 RE	Rocky Mountain Steel	2007	 • Four bolt holes in web (1.25 inch in diameter) • Two electrode pits (B1 and B2) • Crack through entire web thickness emanating from electrode pit to bolt hole (B1)
C	115 RE	Colorado Fuel & Iron	1950's	 • Two electrode pits (C1 and C2) • Two bolt holes in web (1.25 inch in diameter)
D	115 RE	Colorado Fuel & Iron	1950's	 • No bolt holes • One electrode pit (D1)
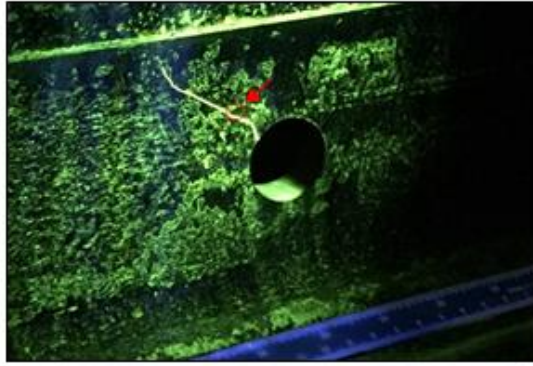
(a) Rail B, Feature B1
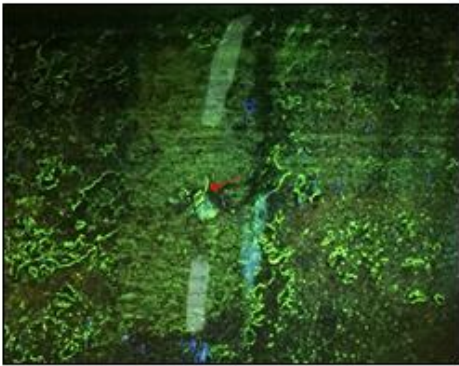
(b) Rail C, Feature C1
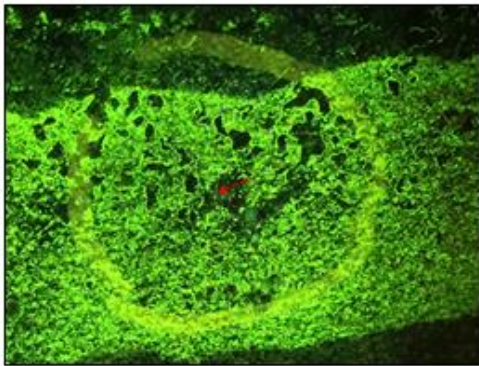
(c) Rail D, Feature D1

**Figure 2: Images from Magnetic Particle Inspection (MPI)**

Metallurgical Analyses

Fractography and metallography provide a metallurgical means to correlate the influence of microstructure to the fracture mode of the material. The most common microstructure of steel used for railroad applications (i.e. rail and wheels) is pearlite. Pearlitic steels are known to have high strength, high hardness, and good wear resistance but low ductility and toughness. Fracture surfaces are examined using optical microscopy, stereomicroscopy, and Scanning Electron Microscopy (SEM). The fracture surfaces may contain topographical features (also referred to as vestigial marks) that are indicative of the manner in which crack extension occurs (i.e. ductile or brittle) leading to ultimate fracture. The examinations of the fracture surfaces combined with additional information from historical usage, mechanical and chemical testing are then used to determine the mode of failure.

The crack in Rail B was broken open in the laboratory to examine the topographical features of the fracture surfaces. Figure 4 shows three photographs of the fracture surface of the crack in Rail B. These photographs provide fractographic evidence indicative of the three stages of fatigue fracture; namely (1) crack initiation or formation originating from the pitting, (2) crack propagation or growth by metal fatigue, and (3) final rupture or fast fracture.

The initiation and fatigue crack growth (or propagation) stages occur over time from cyclic loading. The propagation stage is characterized by the semi-elliptical or thumbnail-shaped crack emanating from the initiation site or the electrode pit, as seen in the far photo of Figure 4. The difference between the maximum and minimum stresses in the cyclic loading plays a significant role in driving the propagation stage. Thermal loads and residual stresses affect the average or mean stress in each cycle. Residual stresses are defined as those that remain in an externally unloaded rail. Residual stresses are created in rail from welding procedures from the non-uniform heating and cooling. Moreover, tensile residual stresses promote the formation and growth of cracks. As propagation continues, the load-bearing capacity of the cracked rail eventually weakens to a point where a single load application (e.g. wheel impact load) may cause sudden rupture, which is characterized as fast fracture in the figure. The role of the thermal load implies that, when the electrode pitting is present, the likelihood of sudden premature rail failure will increase during cold temperatures. This phenomenon is well known and is referred to as the ductile-to-brittle transition.

The cracks identified from the MPI method were then cross sectioned, mounted, and polished for metallurgical analysis. Figure 5 shows photo micrographs of the microstructure near the electrode pits in each rail. These photo micrographs provide further evidence that the origin of the cracking in the rail web is the pitting created from the electrode welding, confirming the hypothesis of electrode-induced web fatigue cracking.
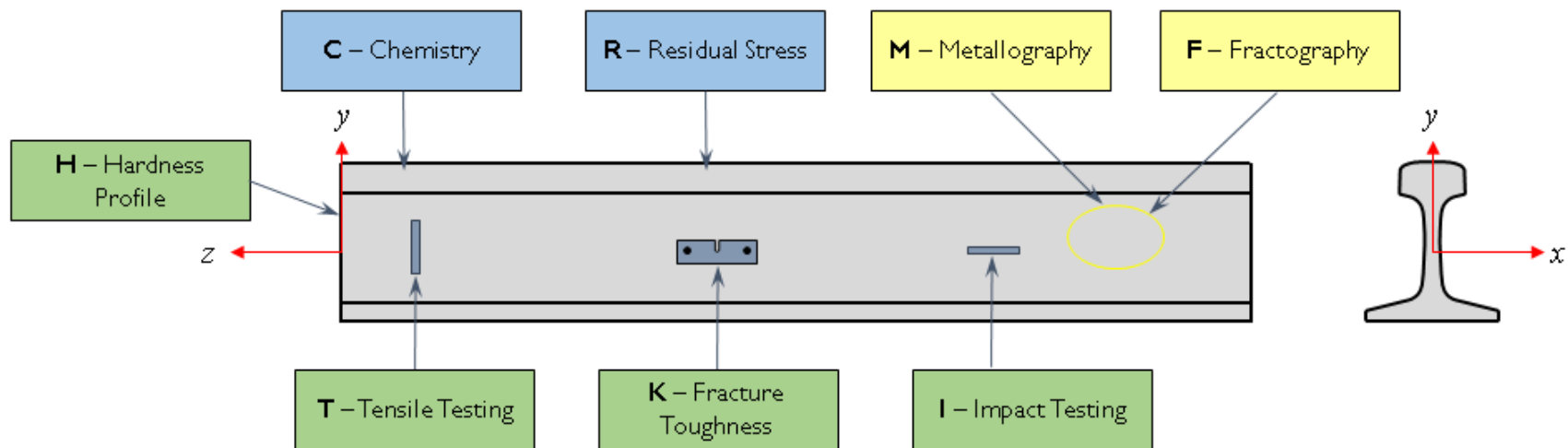
Figure 3: Forensic Evaluations Conducted by Benét Laboratories
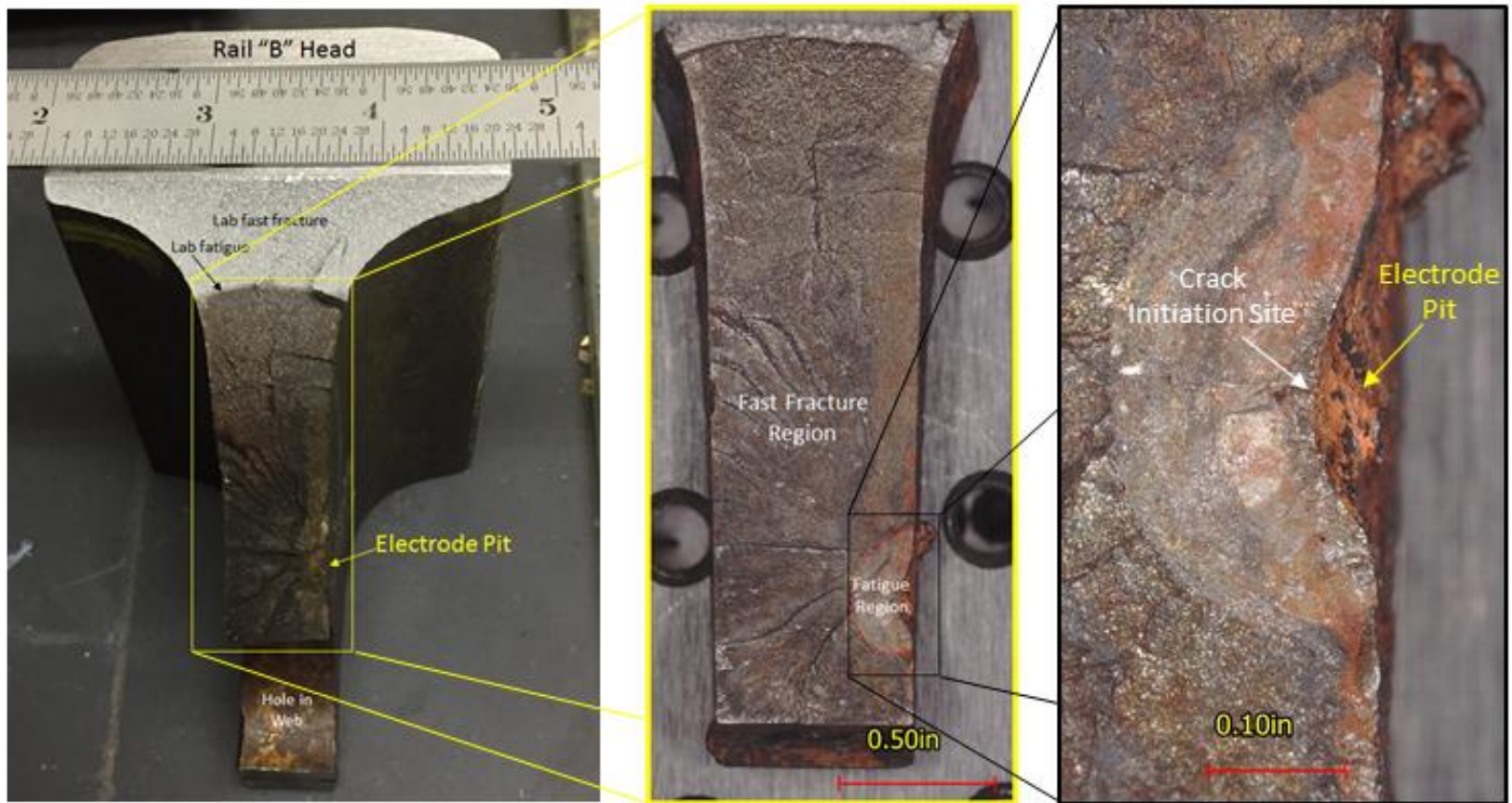
Figure 4: Fracture Surface from Rail B
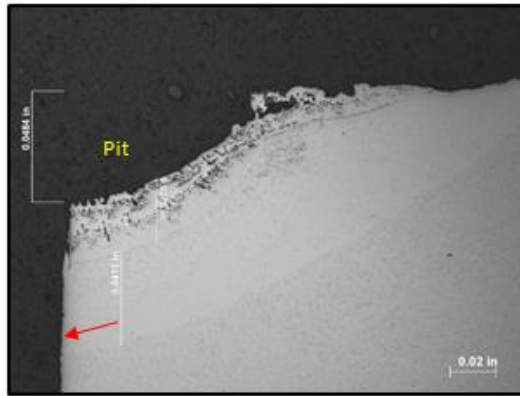
(a) Rail B, Feature B1
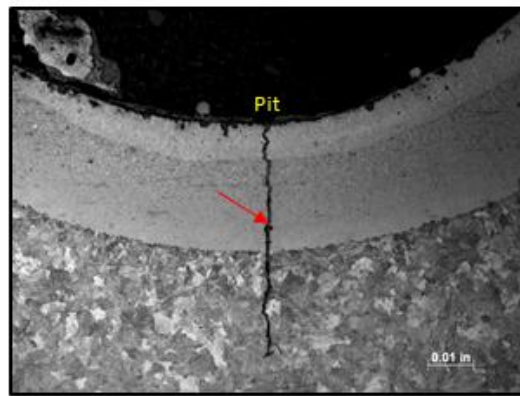
(b) Rail C, Feature C1
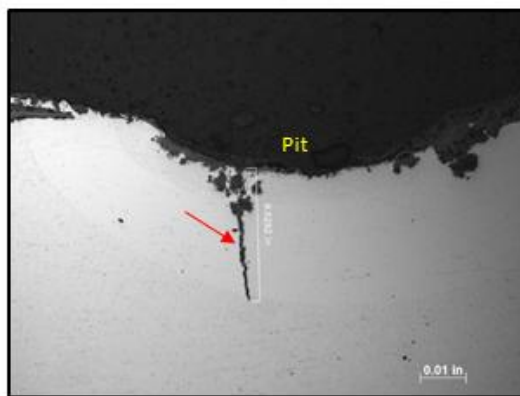
(c) Rail D, Feature D1

Figure 5: Cross Sections of Electrode Pits in Rails B, C, and D.

Evidence of altered microstructure from pearlite to martensite in the heat affected zone was identified in B1 and C1. Martensite transformation occurs from rapid cooling (or quenching) of the steel from high weld temperatures. Steels with martensitic microstructure are known to be extremely hard and fracture-prone. Subsequent reheating of martensite to a temperature below the eutectoid temperature and holding for varying amount of time (called tempering) will produce a strong and tough steel with slightly lower hardness but with much less brittleness [2]. Consequently, tempered martensite is preferable over untempered martensite. The metallurgical analysis of D1 revealed evidence of pitting, cracking, and the formation of a heat affected zone. However, the microstructure of the heat affected zone in D1 remained pearlite.

Chemical Composition

Spark based optical emission spectroscopy was performed by Benét to provide the chemical composition of rails B, C, and D. The results were then compared to specifications published by the American Railway Engineering and Maintenance-of-way Association (AREMA) [3].[2] The AREMA specifications for the chemical content of rail are listed in terms of the following elements: carbon, manganese, phosphorus, sulfur, silicon, nickel, chromium, molybdenum, and vanadium. Moreover, the results from the chemical analysis for each rail, which are listed in Table 2, are within the range of AREMA specifications.

Table 2: Results from Chemical Analysis (wt. %)

Rail ID	C	Mn	P	S	Si	Ni	Cr	Mo	V
B	0.75	1.02	0.008	0.01	0.26	0.07	0.24	0.018	0.004
C	0.71	0.94	0.018	0.03	0.16	0.07	0.03	0.080	0.003
D	0.76	1.03	0.016	0.02	0.29	0.07	0.22	0.016	0005

Mechanical Testing

Mechanical testing performed by Benét comprised: (a) tension testing, (b) hardness profiling, (c) impact testing using Charpy V-notch (CVN) specimens, and (d) fracture toughness testing. All mechanical testing was conducted in accordance to standards published by the American Society for Testing and Materials (ASTM), which are listed in Table 3.

Table 3: ASTM Standards Used for Mechanical Testing

Measurement	ASTM Standard [Reference]
Tensile Properties	E8 [4]
Hardness	E10 [5]
CVN Impact Energy	E23 [6]
Fracture Toughness	E399 [7] and E1820 [8]

---

[2] AREMA is a railway industry group that publishes recommended practices for the design, construction and maintenance of railway infrastructure in the United States and Canada.

Table 4 lists the results from the tensile testing performed on uniaxial specimens taken from Rail B. The table includes the following mechanical properties: Young's modulus (or modulus of elasticity, E), 0.1 percent offset yield strength (0.1%YS), ultimate tensile strength (UTS), percent elongation (%Elong), and percent reduction in area (%RA). The table also notes the minimum AREMA requirements for strength and ductility. Moreover, the measurements for 0.1 percent yield strength, ultimate tensile strength, and percent elongation exceed the AREMA specifications for standard rail steel.[3]

Table 4: Summary of Tensile Test Results on Rail B

Specimen ID	E ($\times10^3$ ksi)	0.1%YS (ksi)	UTS (ksi)	%Elong	%RA
T1	31.1	92.5	165	9.5	27
T2	28.1	96.0	165	12	25
T3	25.8	92.5	165	11	21
T4	29.5	94.5	164	12	30
AREMA	--	70 min.	140 min.	9 min.	--

The average and standard deviation of ten Brinell hardness readings on each rail section are listed in Table 5. The hardness measurements on Rails B and D exceed the AREMA specification (minimum of 300 on the Brinell scale), but the hardness of Rail C was found to be consistently lower (average of 246 HB) than the AREMA minimum. The chemical analysis of Rail C revealed that it had the lowest carbon, silicon, and chromium concentration of the three rails, which may have contributed to its lower hardness. Also, Table 1 indicates that the year of manufacture for Rail C was in the 1950s. Hardness requirements for rail made in that time period may have been lower than today.

Table 5: Summary of Hardness Profiling

Rail ID	Brinell Hardness	
	Average	Standard Deviation
Rail B – End	302	13.5
Rail B – Near Pit	297	11.6
Rail C	246	12.3
Rail D	306	20.6

Charpy V-notch (CVN) testing was conducted on Rail B only to measure impact toughness. Specimens were taken directly from the web of the rail, and were oriented in the y-z plane as shown in Figure 3. Specimens were tested in duplicate at six different temperatures to characterize the ductile-to-brittle transition behavior. Table 6 lists the results from the Charpy V-Notch tests. The test temperature ranged from 0°F to 500°F. AREMA has no specification for impact toughness. The results

from the CVN testing indicate that the ductile-to-brittle transition temperature behavior of Rail B is similar to that of steels with a combination of ferrite and pearlite microstructure[4] and with identical carbon content as fully pearlitic rail steel.

Table 6: Charpy V-Notch Results on Rail B

Specimen ID	Temperature (deg F)	CVN Energy (ft-lb)
C7	0	2
C8	0	2
C1	100	3
C2	100	3
C3	200	6
C4	200	4
C5	300	10
C6	300	10
C9	400	19
C10	400	19
C11	500	19
C12	500	17

Standard fracture mechanics tests were performed to determine fracture toughness more accurately than can be inferred from a Charpy impact test. These tests were performed at room temperature using single-edge bend specimens. The length, height, and thickness of these specimens were 2.30 in. × 0.50 in. × 0.25 in., respectively. In addition, the specimens were side-grooved to provide a V-notch detail of 0.025 in. deep with a 0.010-inch radius in order to promote plane strain conditions. Two orientations of crack extension were evaluated as defined in ASTM E399 [7], and shown schematically in Figure 6.
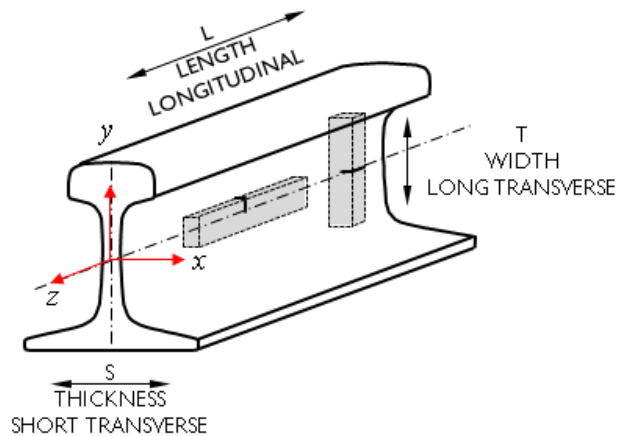

Figure 6: Fracture Toughness Specimen Orientations

---

[3] AREMA has no specifications for the modulus of elasticity and percent reduction in area.

[4] The most common structural steels have a mixed microstructure of ferrite and pearlite. The applications for ferrite-pearlite steels include beams for bridges and high-rise buildings, plates for ships, and reinforcing bars for roadways.

The ASTM E399 standard specifies certain specimen size requirements in order to obtain a valid fracture toughness result. These validity requirements are stipulated to ensure that plane strain conditions exist and that the specimen behaves in a linear elastic manner. Moreover, plane strain conditions are satisfied if the plastic zone ahead of the crack tip is small compared to the thickness of the specimen.

In addition, the loading rate published in ASTM E399 is within the range of 30 to 150 ksi-in$^{1/2}$ per minute. However, previous work reported by Stone [9] demonstrated that the fracture toughness of rail steel is sensitive to loading rate, and tends to decrease as the loading rate increases. In the Benét evaluations, the loading rate was varied and deviated from the ASTM E399 recommended rates in order to assess its effect on fracture toughness.

Table 7 shows the results from eight fracture toughness tests conducted on specimens from Rail D. The table lists the conditional fracture toughness, K_Q and the loading rate in each test. The table also includes two calculations with length dimensions that refer to the specimen size requirements discussed previously. According to ASTM E399, the following specimen size requirement must be met for a valid fracture toughness result:

$$W - a \geq 2.5 \left(\frac{K_Q}{YS} \right)^2$$

As shown by Anderson [10], this size requirement may make it difficult to perform a valid fracture toughness test, unless the material is relatively brittle or the test specimen is very large. With these caveats, the conditional fracture toughness measurements for Rail D may be considered as conservative or lower bound values. By comparison, References [11] and [12] reported average fracture toughness values of rail steel from 35 to 40 ksi-in$^{1/2}$.

Table 7: Fracture Toughness Results on Rail D

	K_Q (ksi-in$^{1/2}$)	Loading Rate (ksi-in$^{1/2}$ per minute)	W-a (inch)	$2.5 \left(\frac{K_Q}{YS} \right)^2$ (inch)	Valid?
L-T 1	31.2	1.0	0.264	0.276	No
L-T 2	39.8	0.7	0.273	0.449	No
L-T 3	30.6	7.4	0.272	0.266	Yes*
L-T 4	27.6	145.5	0.265	0.098	Yes
L-S 1	27.6	0.8	0.261	0.401	No
L-S 2	36.2	0.7	0.268	0.371	No
L-S 3	34.5	6.5	0.267	0.338	No
L-S 4	18.6	137.9	0.270	0.098	Yes

* Meets validity requirement for size but not for loading rate

Although only eight fracture toughness tests were performed, the trend toward lower toughness at faster loading rates is evident and is consistent with the results shown in Figure 7, which is reproduced from Stone [9].
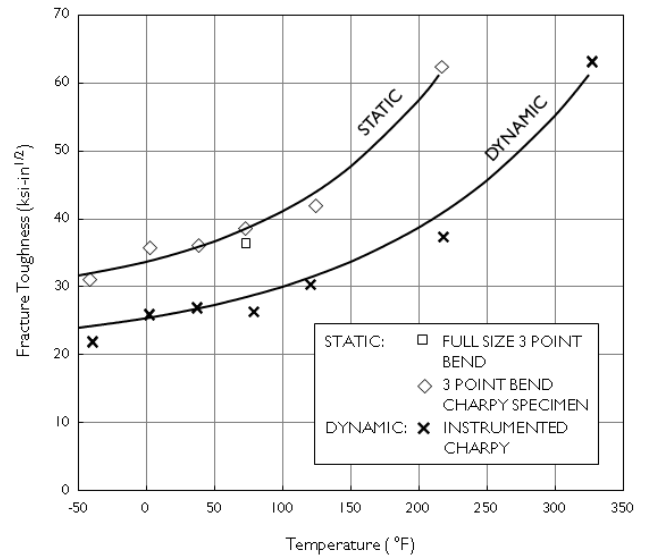

Figure 7: Effect of Temperature and Loading Rate on Fracture Toughness of Rail Steel [9]

Residual Stress Measurements

Welding is known to alter the residual stress state in the parent metal and in the heat affected zone. If the residual stress state is tensile, the fatigue crack growth stage will accelerate. Conversely, compressive residual stresses will tend to retard the growth of fatigue cracks. Previous research on the various methods to measure residual stresses in rail is described in Reference [13].

The Inter-agency Agreement between Volpe and Benét included the nondestructive measurement of residual stresses in the vicinity of (and away from) the electrode pits using a method called X-ray diffraction (XRD). Moreover, the measurement of residual stresses may provide insight on the nature, magnitude, and distribution of the residual stresses produced from pressure electric welding.

Residual stress measurements were made on Rail D only at three different locations along the vertical axis of the rail web. Profiling was performed at each vertical location in order to measure residual stress as a function of depth. Moreover, testing was performed remote from any electrode pitting damage.

The average of the minimum and maximum residual stress measurements at the three locations are shown in Figure 8. The figure also shows that the measurements from the XRD method are generally consistent with the range of longitudinal residual stress measurements reported in previous research by Wineman [14].
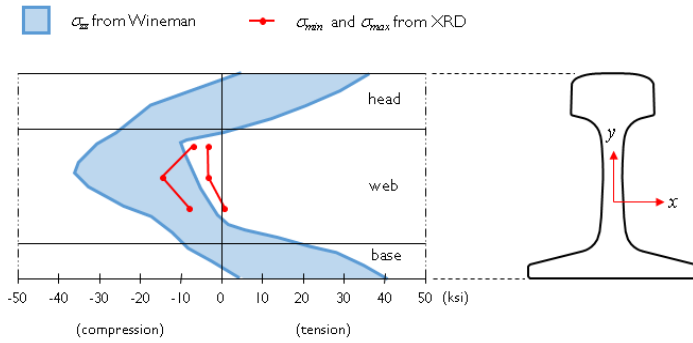
Figure 8: Comparison of Residual Stress Measurements

Figure 9: Transverse Defect and Potential Electrode Pitting in Rail Head

DISCUSSION AND FOLLOW-UP

Results from the testing for chemical composition, and mechanical properties were shown to be within or exceed the specifications published by AREMA. Moreover, the results from these particular tests indicate that inadequate material can be ruled out as a cause of pre-mature cracking. In addition, residual stress measurements were shown to be consistent with those from previous results in the rail web.

Results from the fractographic and metallographic analyses provided evidence that fatigue cracks in the web are the result of pitting caused by inadequate electrode-to-rail contact. These results also substantiate a school of thought regarding the integrity of rail welds that the welder determines the ultimate fate of the weld when it is installed. If the weld is installed properly, it stands a better chance of performing well in service. However, improper installation can lead to fatigue cracking and premature rail failure.

These results were presented to the Rail Integrity Working Group of the Railroad Safety Advisory Committee (RSAC) in May 2017. Subsequently, electrode-induced pitting from pressure electric welding was observed on railroads other than those who provided rails to FRA for the Benét evaluations. Furthermore, electrode pitting was observed to occur in the head of the rail. Apparently, pressure electric welds made in the plant use heads that clamp onto the rail ends on top (i.e. running surface) and bottom of the rail. Figure 9 is a photograph of a rail with a transverse defect originating at the center of the head. The location of the transverse defect is consistent with the location in which electrode pitting may potentially occur. Additional rails with transverse defects in the rail head were sent to Benét for evaluations similar to those conducted on the rails with electrode pitting on the web. These additional evaluations had not yet been completed when this paper was being prepared.

CONCLUDING REMARKS

The Benét evaluations described in this paper provided forensic evidence confirming FRA's hypothesis that electrode-induced web fatigue cracking is the result of pitting caused by inadequate electrode-to-rail contact during pressure electric welding.

Based on these findings, FRA's Office of Railroad Safety published a notice of FRA's intent to issue a Safety Advisory to alert railroads, contractors, and the rail welding industry of the potential for electrode-induced rail pitting and fatigue cracking during the pressure electric welding process [15]. The Safety Advisory also includes recommendations to help the industry prevent electrode-induced rail pitting and to inspect for and then remediate such pitting if it occurs.

ACKNOWLEDGMENTS

REFERENCES

1. Vigilante, G.N., Ethier, C.L., and Troiano, E.J., "Evaluation of Railroad Rails Containing Electrode Pits," U.S. Army Benét Laboratories Report, March 2017.
2. Campbell, F.C., *Phase Diagrams – Understanding the Basics,* ASM International, 2012.
3. Manual for Railway Engineering, American Railway Engineering and Maintenance-of-Way Association (AREMA) Manual, Part 2 – Manufacture of Rail, 1999.
4. ASTM Standard E8, "Standard Test Methods for Tension Testing of Metallic Materials," ASTM International, 2016.
5. ASTM Standard E10, "Standard Test Methods for Brinell Hardness of Metallic Materials," ASTM International, 2015.

6. ASTM Standard E23, "Standard Test Methods for Notched Bar Impact Testing of Metallic Materials," ASTM International, 2016.

7. ASTM Standard E399, "Standard Test Method for Linear-Elastic Plane-Strain Fracture Toughness, K_{IC} of Metallic Materials," ASTM International, 2012.

8. ASTM Standard E1820, "Standard Test Method for Measurement of Fracture Toughness," ASTM International, 2011.

9. Stone, D.H., "An Introduction to the Fracture Mechanics of Railroad Rails," *Proceedings of the Symposium on Railroad Track Mechanics*, Pergamon Press, 1975, pp. 353-368.

10. Anderson, T.L., *Fracture Mechanics – Fundamentals and Applications*, 3rd edition, CRC Press, 2005.

11. Orringer, O., et al., "Crack Propagation Life of Detail Fractures in Rails," Volpe Center Final Report to Federal Railroad Administration, DOT/FRA/ORD-88-13, October 1988.

12. Ölund, P., "Crack Propagation Properties and Fracture Toughness in Rail Steel – A Literature Review," NTIS Report PB95258539, October 1994.

13. Orringer, O., Orkisz, J., and Swiderski, Z., *Residual Stresses in Rails, Volume 1: Field Experience and Test Results*, Kluwer Academic Publishers, Dordrecht, 1992.

14. Wineman, S.J., "Residual stresses and web fracture in roller-straightened rail," Ph.D. Thesis, Department of Mechanical Engineering, Massachusetts Institute of Technology, Cambridge, MA, June 1991.

15. Docket No. FRA-2017-0074, "Addressing Electrode-Induced Rail Pitting From Pressure Electric Welding," *Federal Register,* Vol. 82, No. 157, August 16, 2017, pp. 38989-38992.